37 pixel Camera. (Inner 19)

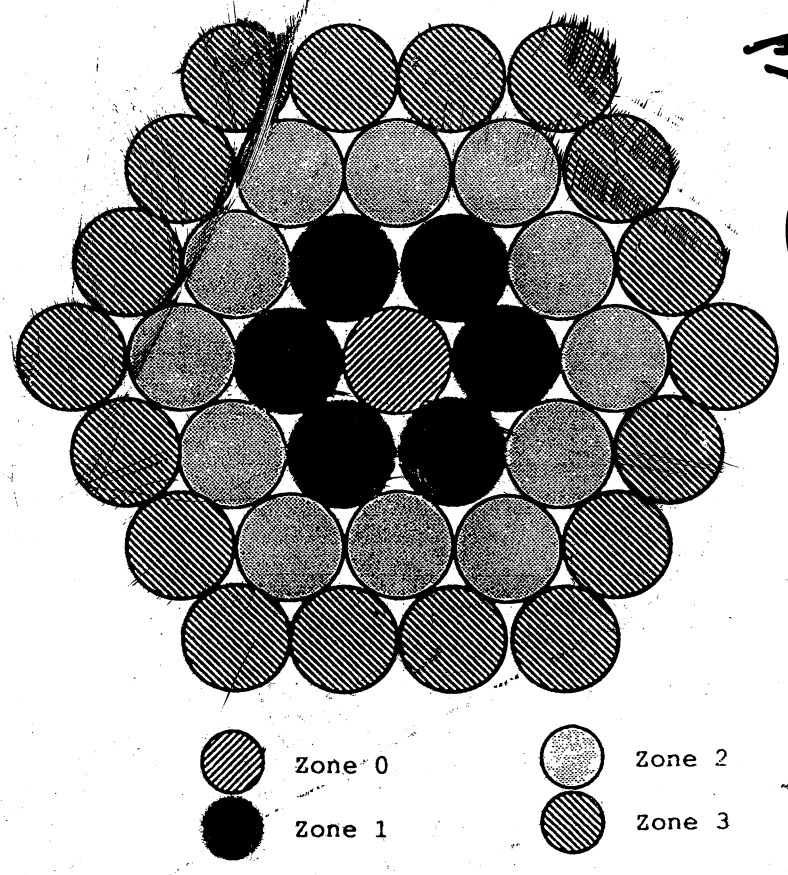

FIG. 1.—Layout of phototubes in the focal plane of the 10 m optical reflector. Each phototube has a sensitive area defined by a diameter of 0°.5, the spacing between phototubes is 0°.5. The full field of view is 3°.5. The center phototube is defined as zone 0; the surrounding ring of six phototubes is zone 1, the ring of 12 zone 2, and the outer ring of 18 zone 3. The latter is not included in the camera trigger.

the dark night sky. Although this system adds noise to each channel, it is considered essential if stable trigger conditions are to be maintained between the ON and OFF regions. Because the 10 m reflector is on an altazimuth mount, the star field slowly rotates as the source is tracked sidereally. The presence of a bright star ($m_v < +3.0$) in the field of view may exceed the padding lamp's ability to compensate for the changing light level in a particular phototube. If so, that phototube is turned off for the duration of the ON and OFF scans.

Typically the trigger rate in each channel was 1 Hz, and the event trigger rate was 3–4 Hz at the zenith. The latter had a zenith angle dependence that went as $R_z = R_0 \cos^{-2.5} z$, where R_0 is the rate at the zenith and z is the zenith angle. The random rate from night-sky fluctuations was negligible, but there was a small zenith-angle-dependent contribution to the trigger rate from cosmic-ray particles physically passing through two or more adjacent phototubes in the focus box. This rate was measured to be 0.01–0.03 Hz.

The above limits the accuracy with which the shower image characteristics can be measured. There are three types of noise present in the recorded pulse heights: (1) shot noise in the signal itself; (2) noise due to fluctuations in the night-sky-light (plus padding lamp), which is also a form of shot noise; (3) pickup, electronic noise, etc., downstream of the phototubes. The latter was found to be negligible.

Under operating conditions (dark night sky) the average current in each phototube is 0.33 photoelectron per nsec. The night-sky noise is effectively the fluctuation in this number within the 45 nsec integration time of the camera. Artificial triggers of the camera permitted this number to be measured; the result is ~5.9 photoelectrons per channel per gate width. The minimum possible is 3.9 photoelectrons, which is the Poisson standard deviation in the number of photoelectrons emitted by the photocathode. Thus we find a value 1.5 times the Poisson value.

Shot noise in the signal itself was measured by consideration of the fluctuations when the camera is triggered by a pulsed nitrogen discharge tube which uniformly illuminates each phototube (Lewis *et al.* 1987). These nitrogen flash images indicated that the measured signals show fluctuations that are 1.3 times the expected Poisson deviation, in approximate agreement with value derived above. These results are consistent with the expected noise due to the statistics of the dynode secondary emission process.

Absolute calibration of the camera is based upon consideration of the above noise levels and from a direct measurement using a calibrated radioactive light source on the face of each phototube. The light source was calibrated using an acrylic Cerenkov muon telescope (Gorham 1986). These measurements indicated a conversion factor of 1.4 photoelectrons per digital count. The trigger level for each of the 19 inner tubes was ~50 electrons.

c) Observations

The ON/OFF tracking technique was generally used for the observations of the Crab Nebula. The typical procedure was to

today - 4 - 12 m. mirrors 499 pmts - 3.5° FOV

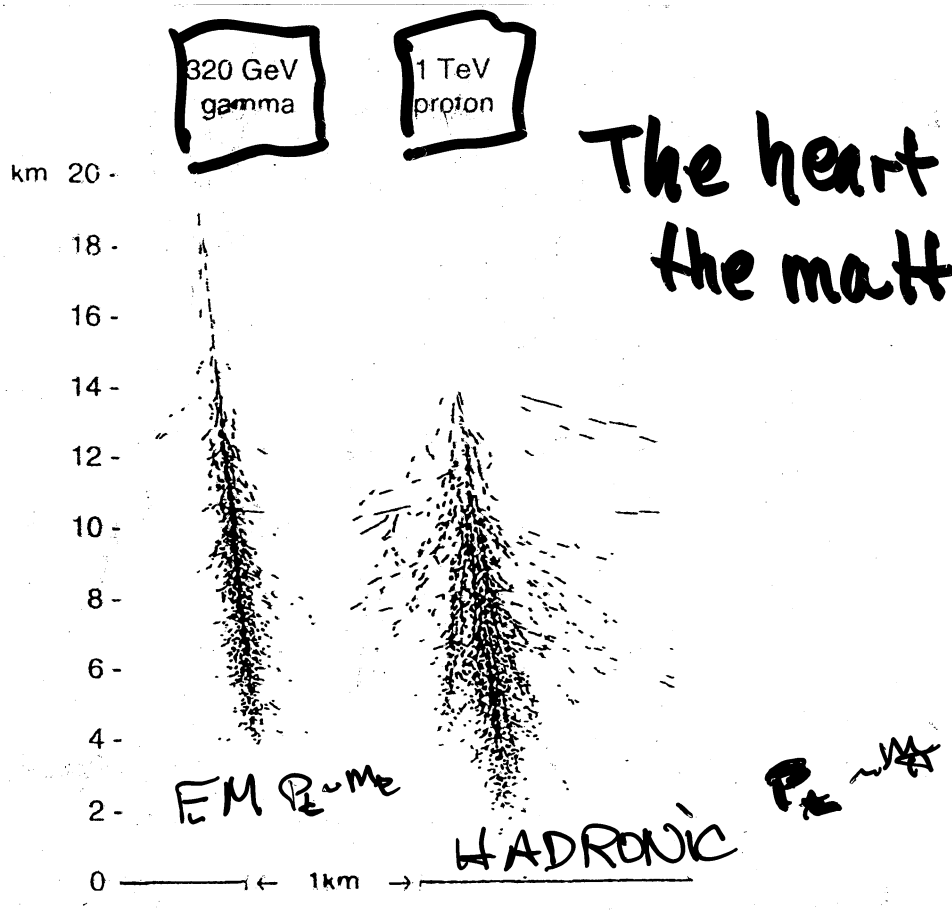

Fig. 1. Different form of showers generated by gamma-rays and protons. On the left, a 320 GeV gamma shower; on the right a 1 TeV proton. The lateral scale is exaggerated by a factor 5. The picture is thinned down by showing each track as a sparsely dashed line.

in points of emission of Čerenkov photons – is somewhat different in the two cases: proton showers have a longer penetrating tail, some particles reaching the ground and giving a more intense Čerenkov radiation near the shower axis. Figure 3 shows the average distribution in atmospheric depth of the emitted light, but omitting light emitted directly by muons. The muons, in proton showers, do penetrate to the ground over a wide area, and an intense local peak of Čerenkov light is seen around each muon impact point. Proton showers show much greater shower-to-shower fluctuations in longitudinal profile than do gamma showers. Figure 4 illustrates typical cases (again omitting the more widely spread muon "tail", to make the point that even the core electron-photon cascades differ for the two types of shower). These differences in longitudinal profile will not, however, identify every proton shower. Showers due to heavy nuclei of the cosmic radiation are even more well distinguished from gamma showers. For the same energy, they are even more laterally diffuse, and contain more muon tracks, contributing to patchy muon light (at TeV energies).

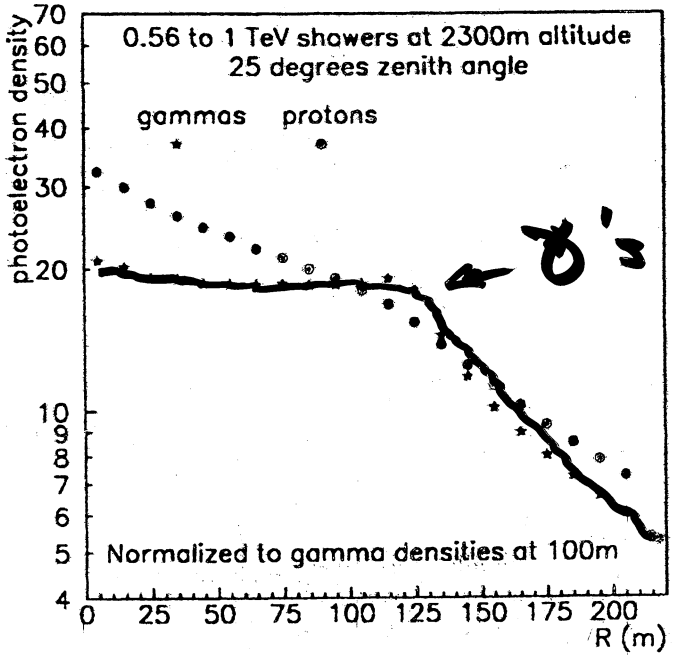

Fig. 2. Average lateral distributions of Čerenkov light at about 700 GeV

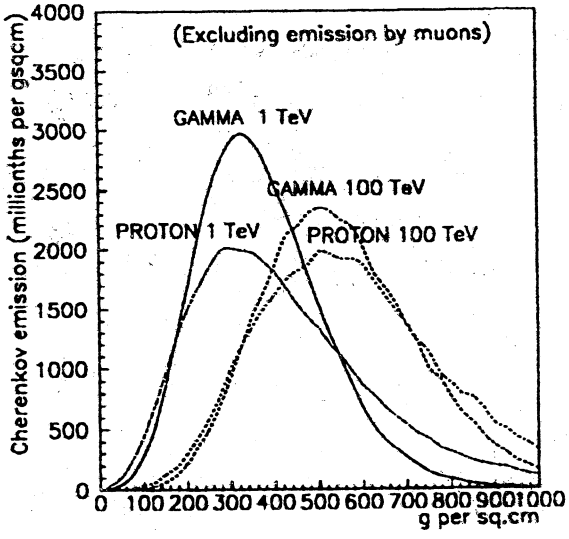

Fig. 3. Average longitudinal distribution of Čerenkov emission

2.1. Main characteristics of Čerenkov light from showers

Figure 5 shows schematically the anatomy of Čerenkov light in a shower.

Figure 2, below, shows the distribution of the widths, lengths, and other parameters of background proton showers, and for showers from oxygen

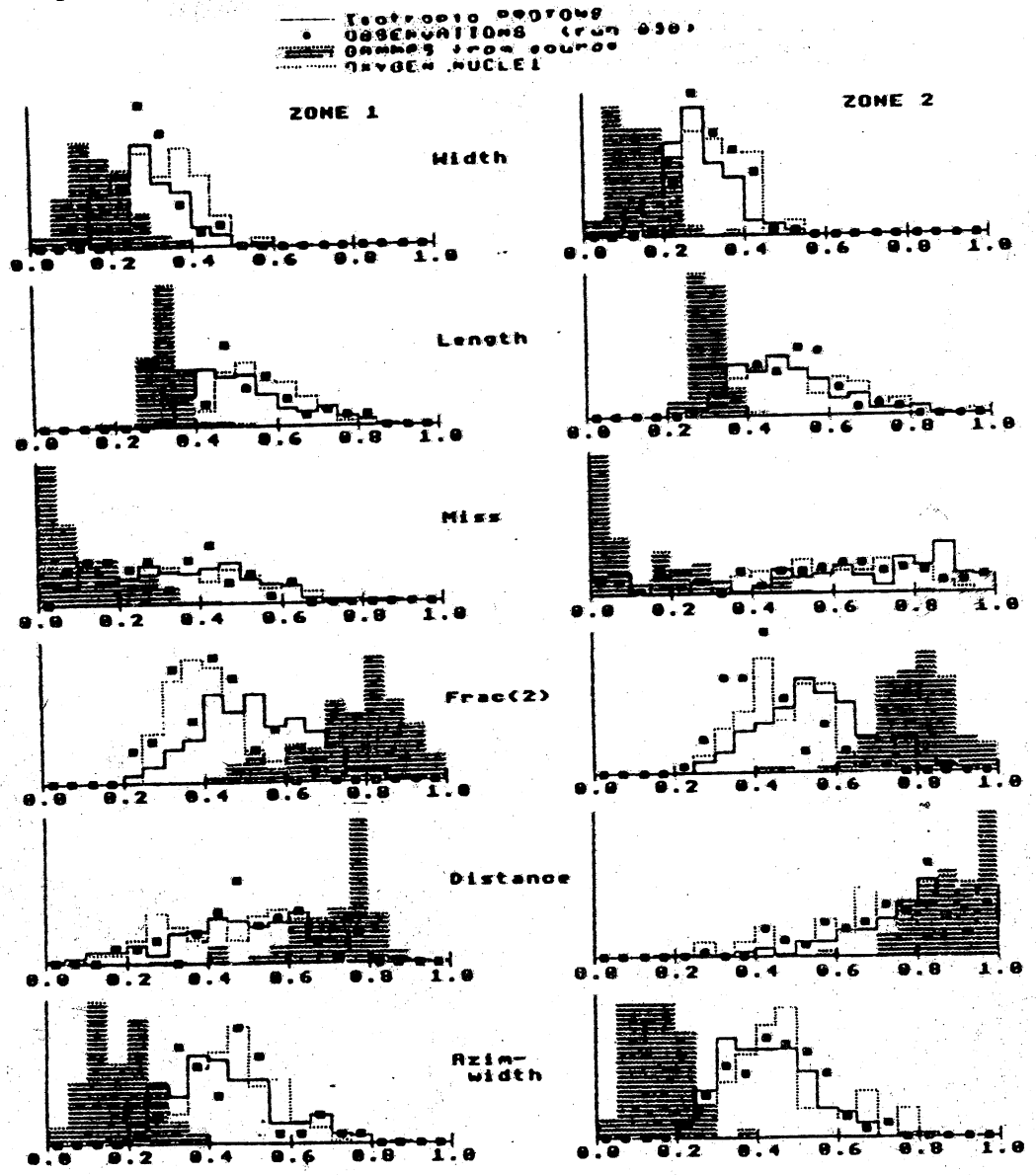

Figure 2: histograms of image characteristics. (vertical showers) nuclei, compared with those for gamma-ray showers (shaded histogram) from a source placed in the centre of the field of view. Units: degrees — except for *FRAC(2)*, which is dimensionless. The triggering requirement is

netic in nature and are most likely gamma rays.

Ireland. A. M. H. and T. C. W. acknowledge the support of a NATO grant.

4

APPENDIX

Suppose the ith phototube is given coordinates x_i, y_i (in degrees) and registers a signal s_i. The origin of the coordinates will be the center of the array of phototubes. The axis of an image is expressed by the equation:

$$y = ax + b .$$

Then defining (as usual)

$$\langle x \rangle = \Sigma_i s_i x_i / \Sigma_i s_i , \qquad \langle x^2 \rangle = \Sigma_i s_i x_i^2 / \Sigma_i s_i , \qquad \langle y \rangle = \Sigma_i s_i y_i / \Sigma_i s_i ,$$
$$\langle y^2 \rangle = \Sigma_i s_i y_i^2 / \Sigma_i s_i , \qquad \langle xy \rangle = \Sigma_i s_i y_i / \Sigma_i s_i ,$$

and

$$S_x^2 = \langle x^2 \rangle - \langle x \rangle^2 , \qquad S_y^2 = \langle y^2 \rangle - \langle y \rangle^2 , \qquad S_{xy} = \langle xy \rangle - \langle x \rangle \langle y \rangle .$$

If $d = S_y^2 - S_x^2$, then

$$a = \{ d + \sqrt{[d^2 + 4(S_{xy})^2]} \} / 2S_{xy} , \qquad b = \langle y \rangle - a \langle x \rangle ,$$
$$(width)^2 = (S_y^2 + a^2 S_x^2 - 2aS_{xy})/(1 + a^2) , \qquad (length)^2 = (S_x^2 + a^2 S_y^2 + 2aS_{xy})/(1 + a^2) ,$$
$$miss = ABS[(b)/\sqrt{(1 + a^2)}] , \qquad dis = r = \sqrt{(\langle x \rangle^2 + \langle y \rangle^2)} .$$

(NOT the shower impact parameter!).

To obtain the azimuthal width (*azwidth*), we first transform to coordinates (p, q) aligned along and perpendicular to the radial direction to the centroid. Then if

$$\sin \theta = \langle y \rangle / r \quad \text{and} \quad \cos \theta = \langle x \rangle / r ,$$
$$q = (\langle x \rangle - x) \sin \theta + (y - \langle y \rangle) \cos \theta .$$

Then *azwidth* is the rms spread in q:

$$(azwidth)^2 = \langle q^2 \rangle - \langle q \rangle^2 ,$$

the means being weighted by the signal in the phototube at coordinate (p, q), as in the original calculation of $\langle x \rangle$, etc.

REFERENCES

Ash, M. E., Shapiro, I. I., and Smith, W. B. 1967, *A.J.*, 72, 338.
Bhat, P. N., Ramana Murthy, P. V., Sreekantan, B. V., and Vishwanath, P. R. 1986, *Nature*, 319, 127.
———. 1987, *Proc. 20th Internat. Cosmic Ray Conf.* (*Moscow*), 1, 270.
Boone, J., Cady, R., Cassiday, G. L., Elbert, J. W., Loh, E. C., Sokolsky, P., Steck, D., and Wasserbaech, S. 1984, *Ap. J.*, 285, 264.
Cawley, M. F., *et al.* 1985*a*, *Proc. 19th Internat. Cosmic Ray Conf.* (*La Jolla*), (NASA CP-2376) 1, 131.
———. 1985*b*, in *Proc. 19th Internat. Cosmic Ray Conf.* (*La Jolla*), (NASA CP-2376) 3, 453.
———. 1985*c*, *Ap. J.*, 296, 185.
———. 1987, *Proc. 20th Internat. Cosmic Ray Conf.* (*Moscow*), 1, 240.
Clear, J., Bennett, K., Buccheri, R., Grenier, I. A., Hermsen, W., Mayer-Hasselwander, H. A., and Sacco, B. 1987, *Astr. Ap.*, 174, 85.
Craig, M. A. B., Orford, K. J., Turver, K. E., and Weekes, T. C. 1981, *Proc. 17th Internat. Cosmic Ray Conf.* (*Paris*), 1, 3.
Davies, J. M., and Cotton, E. S. 1957, *J. Solar Energy, Sci. Eng.*, 1, 16.
Dowthwaite, J. C., Harrison, A. B., Kirkman, I. W., Macrae, H. J., McComb, T. J. L., Orford, K. J., Turver, K. E., and Walmsley, M. 1984, *Ap. J.* (*Letters*), 286, L35.
Dzikowski, T., Gawin, J., Grochalska, B., and Wdowczyk, J. 1981, *Phil. Trans. Roy. Soc. London*, *A*, 301, 641.
Erickson, R., Fickle, R., and Lamb, R. C. 1976, *Ap. J.*, 210, 539.
Fazio, G. G., Helmken, H. F., O'Mongain, E., Rieke, G. H., and Weekes, T. C. 1972, *Ap. J.* (*Letters*), 175, L117.
Fegan, D. J., McBreen, B., O'Mongain, E., Porter, N. A., and Slevin, P. J. 1968, *Canadian J. Phys.*, 46, S433.
Gibbs, K. 1987, Ph.D. thesis, University of Arizona.
Gibson, I. A., Harrison, A. B., Kirkman, I. W., Lotts, A. P., Macrae, J. H., Orford, K. J., Turver, K. E., and Walmsley, M. 1982*a*, *Nature*, 296, 833.
———. 1982*b*, in *Proc. Workshop on Very High Energy Gamma-Ray Astronomy*, ed. P. V. Ramana Murthy and T. C. Weekes (Bombay: Tata Institute), p. 97.
Gorham, P. W. 1986, Ph.D. thesis, University of Hawaii.
Gorham, P. W., *et al.* 1986*a*, *Ap. J.*, 309, 114.
———. 1986*b*, *Ap. J.* (*Letters*), 308, L11.
Gould, R. J. 1965, *Phys. Rev. Letters*, 15, 511.
Grenier, I. A., Hermsen, W., and Clear, J. 1987, *Proc. 20th Internat. Cosmic Ray Conf.* (*Moscow*), 1, 77.
Grindlay, J. E. 1971, *Smithsonian Ap. Obs. Spec. Rept.*, No. 334.

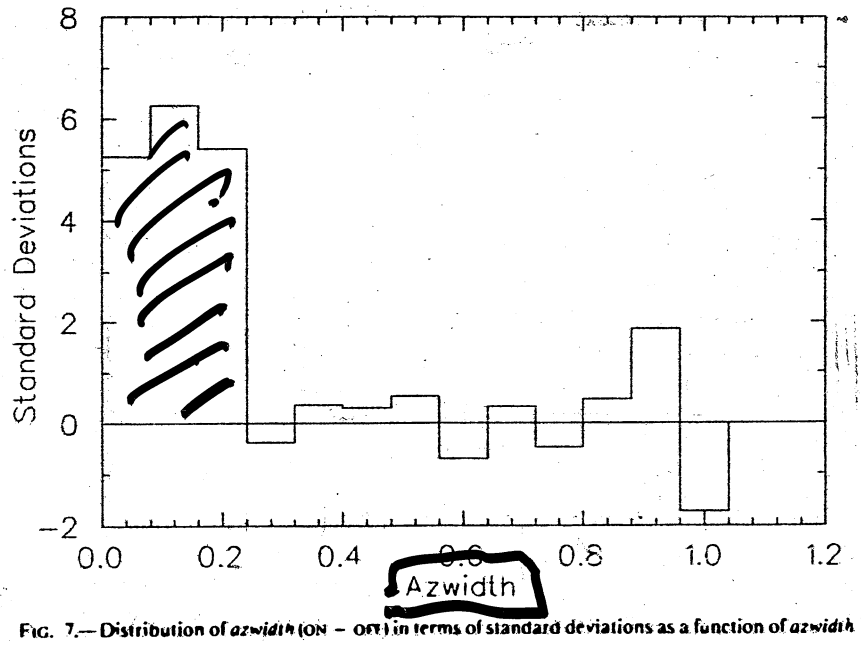

FIG. 7.—Distribution of *azwidth* (ON − OFF) in terms of standard deviations as a function of *azwidth*

ment of the shower and is hence quite different from *width* which is a strong function of the lateral spread. That it provides independent discrimination is an important confirmation of the photonic nature of the primary radiation. *Conc* is a combination of *width* and *length* and hence is not independent. *Dis* is the weakest discriminator in the simulations. This is seen to be the case here also (Table 6). When a combination of parameters is used, e.g., when four of the six parameter cuts are satisfied (as suggested by Hillas 1985), the effect is of comparable significance with the use of *azwidth* alone. An empirical selection (four out of five), with *dis* excluded, is even more significant ($+8.45\ \sigma$).

b) *Previous Observations*

In an early version of the camera (Clear *et al.* 1983; Cawley *et al.* 1985*b*), we made a series of observations of the Crab Nebula using basically the same technique. A total of 82 ON/OFF scans were made using the same observing technique as analysis. These observations were made prior to the detailed simulations with their prediction of distinct gamma-ray domains (Hillas 1985); however, an analysis based on an empirically defined parameter, *frac*(*2*) (now renamed *conc*), designed to exploit the difference between the measured angular size of Cerenkov light images and the simulated size of *gamma-ray* images, gave an excess of events from the direction of the Crab Nebula of 3–4 σ (Cawley *et al.* 1985*a*). An absolute significance could not be assigned to this excess since the separation into gamma-ray and background domains was empirically derived.

After the publication of the detailed simulations, this same data base was analyzed using the predicted discrimination factors (Gibbs 1987). The results are shown in Table 7. Although the statistical significance is not high, the results were sufficiently encouraging to warrant further observations using the upgraded camera.

Since there were significant differences between this

TABLE 4

Azwidth DISCRIMINATION

Epoch	ON	OFF	All (%)	Difference	OFF (%)	Significance
No Selection (All)						
1986–1988.....	652,974	651,801	100.0	+1173	0.2	+1.03
Azwidth Selection						
1986–1988.....	9092	7929	1.2	+1163	14.7	+8.91

We note that (*a*) the percentage of events that are rejected by the *azwidth* discrimination threshold is greater than 98%, in agreement with the simulations (Hillas 1985); (*b*) there is an excess of candidate gamma-ray events in the ON source data of order 15%; (*c*) the effect is consistent with the difference in the "all" ON/OFF pairs, i.e., the selection has not rejected many gamma-ray events; (*d*) a significant excess is only seen when gamma-ray–like events are selected, so that there can be little doubt about the nature of the primary that causes the excess; (*e*) the cumulative total excess has a statistical significance of 8.9 σ; this is a level not generally encountered in very high energy or ultra-high energy gamma-ray astronomy.

The overall distribution of *azwidth* parameters for the ON and OFF scans (for $z < 30°$) are shown in Figure 6. Also shown is the difference in detail for *azwidth* less than 0°.35; this should be compared with Figures 4 and 5. Within the statistical limitations of the simulations (which were performed only for $z = 0°$) there is good qualitative agreement. We have also [illegible] the differences in the two *azwidth* distributions over [illegible]e for possible anomalies; these are plotted in [illegible] (ON − OFF) in standard deviations as a function of *azwidth*. It is apparent that the only significant differences are at small values of *azwidth*.

In Figure 8*a* we have plotted the distribution of individual (ON − OFF) effects (in standard deviations) in the 175 pairs using the *azwidth* canonical cut. To check on the run-to-run stability of the *azwidth* distributions we have also shown the distribution of (ON − OFF) effects using a cut at *azwidth* > 0°.7 (chosen to pass approximately the same number of events as the canonical cut passes at the other end of the distribution; i.e., ON = 15,163, OFF = 15,066, ON − OFF = 97 [+0.56 σ]). It is apparent that the distributions are within statistics apart from a net positive displacement in the canonical cut distribution. For comparison, we also show the same two distributions for 36 ON/OFF pairs of a control data set (discussed below) in Figure 8*b*.

ii) *Width and Miss Correlation*

Both the image shape and orientation discrimination contribute to the effect seen in *azwidth*, as is apparent in Table 5, in which the effect is also broken down by observing season.

iv) *Multiple Parameter Selection*

A net excess from the source direction is seen when discrimination is based on any one of the three parameters, *length, conc, or dis. Length* is a measure of the longitudinal develop-

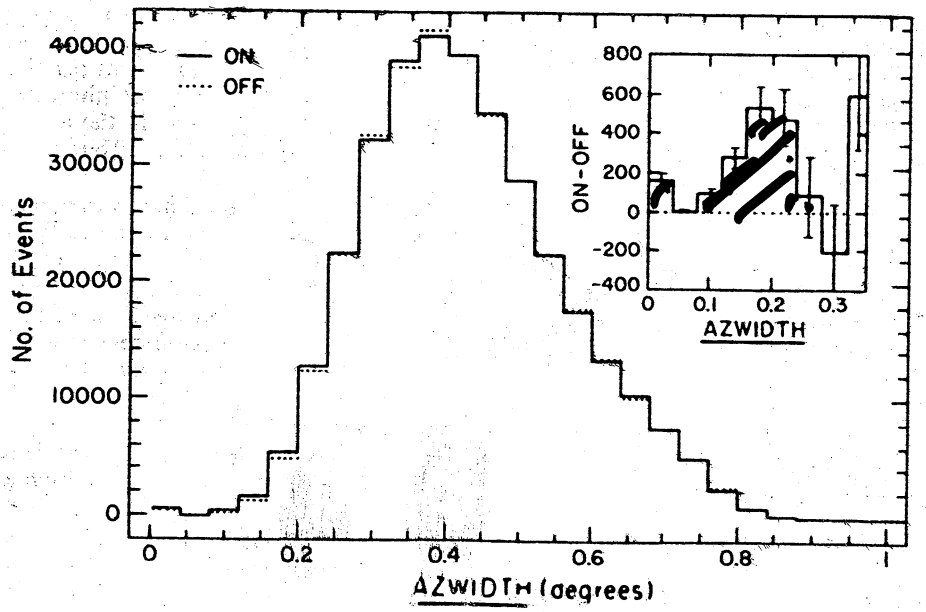

FIG. 6.—Distribution of "all" ON and OFF *azwidth* parameters (with $z < 30°$) for image zones 1 and 2 combined, with the differences in the two distributions in the gamma-ray domain shown in the inset.

Typical Raw Image

7

(a) Typical recorded event

		23	29	27	109	
	20	17	36	90	21	
14	22	36	90	25	21	
18	24	28	43	22	26	23
17	17	21	14	20	24	
	18	24	18	21	16	
		22	23	23	15	

(b) After Calibration

After Calibration

		1.5	6.0	0.0	100.9	
	1.8	-3.5	15.9	114.6	15.7	
-3.6	-0.4	16.2	71.8	4.5	-0.2	
-2.3	2.2	7.7	23.8	1.2	5.1	2.0
-7.4	-4.1	0.5	-5.9	1.1	2.6	
	-1.8	4.5	-2.9	0.9	-5.4	
		2.4	2.1	1.2	-9.6	

(c) After Noise Reduction

Cleaning

		0.0	0.0	0.0	100.9	
	0.0	0.0	15.9	114.6	15.7	
0.0	0.0	16.2	71.8	0.0	0.0	
0.0	0.0	0.0	23.8	0.0	0.0	0.0
0.0	0.0	0.0	0.0	0.0	0.0	
	0.0	0.0	0.0	0.0	0.0	
		0.0	0.0	0.0	0.0	

(d) Parameters derived from image.

Image Zone 2. Zenith Angle=35.32°.

Parameter.	Image value.	Gamma-ray Domain.	Result.
WIDTH	0.15°	< 0.14°	Fail
LENGTH	0.47°	< 0.30°	Fail
MIS	0.13°	< 0.22°	Pass
CONC	0.60	> 0.79	Fail
AZWIDTH	0.16°	< 0.18°	Pass
DIS	0.94°	> 0.84°	Pass
4/6			Fail

FIG. 2.—Typical image shown at various stages in the image processing: (*a*) raw image; (*b*) after pedestal subtraction and gain normalization; (*c*) after subtraction of subthreshold signal channels; (*d*) image parameters derived from (*c*), using the methods outlined in the appendix, and limits of gamma-ray domain.

2013

DISCOVERY OF A NEW TeV GAMMA-RAY SOURCE: VER J0521+211

S. [illegible]BAULT[1], T. ARLEN[2], T. AUNE[2], B. BEHERA[3], M. BEILICKE[4], W. BENBOW[5], R. BIRD[6], A. BOUVIER[7], J. H. BUCKLEY[4], V. [illegible][4], K. BYRUM[8], A. CESARINI[9], L. CIUPIK[10], M. P. CONNOLLY[9], W. CUI[11], M. ERRANDO[12], A. FALCONE[13], S. FEDERICI[3,14], Q. FENG[11], J. P. FINLEY[11], L. FORTSON[15], A. FURNISS[7], N. GALANTE[5], D. GALL[16], G. H. GILLANDERS[9], S. GRIFFIN[1], J. GRUBE[10], G. GYUK[10], D. H[illegible][1], J. H[illegible][17], G. HUGHES[3], T. B. HUMENSKY[18], P. KAARET[16], M. KERTZMAN[19], Y. KHASSEN[6], D. KIEDA[20], H. KRAWCZYNSKI[3], F. [illegible]NRICH[21], S. KUMAR[17], M. J. LANG[9], A. S MADHAVAN[21], G. MAIER[3], P. MAJUMDAR[2,22], S. MCARTHUR[23], A. MCCANN[24], J. MILLIS[25], P. MORIARTY[26], R. MUKHERJEE[12], A. O'FAOLÁIN DE BHRÓITHE[6], R. A. ONG[2], A. N. OTTE[27], N. PARK[23], J. S. PERKINS[28], M. POHL[3,14], A. POPKOW[2], H. PROKOPH[3], J. QUINN[6], K. RAGAN[1], L. C. REYES[29], P. T. REYNOLDS[30], G. T. RICHARDS[27], E. ROACHE[5], D. B. SAXON[17], G. H. SEMBROSKI[11], A. W. SMITH[20], D. STASZAK[1], I. TELEZHINSKY[3,14], M. THEILING[11], A. VARLOTTA[11], V. V. VASSILIEV[2], S. VINCENT[3], S. P. WAKELY[23], T. C. WEEKES[5], A. WEINSTEIN[21], R. WELSING[3], D. A. WILLIAMS[7], B. ZITZER[8]

(THE VERITAS COLLABORATION)

AND

M. BÖTTCHER[31], S. J. FEGAN[32], P. FORTIN[5], J. P. HALPERN[33], Y. Y. KOVALEV[34,35], M. L. LISTER[36], J. LIU[33], A. B. PUSHKAREV[37,38], AND P. S. SMITH[39]

[1] Physics Department, McGill University, Montreal, QC H3A 2T8, Canada
[2] Department of Physics and Astronomy, University of California, Los Angeles, CA 90095, USA
[3] DESY, Platanenallee 6, D-15738 Zeuthen, Germany
[4] Department of Physics, Washington University, St. Louis, MO 63130, USA
[5] Fred Lawrence Whipple Observatory, Harvard-Smithsonian Center for Astrophysics, Amado, AZ 85645, USA; fortin@veritas.sao.arizona.edu
[6] School of Physics, University College Dublin, Belfield, Dublin 4, Ireland
[7] Santa Cruz Institute for Particle Physics and Department of Physics, University of California, Santa Cruz, CA 95064, USA
[8] Argonne National Laboratory, 9700 S. Cass Avenue, Argonne, IL 60439, USA
[9] School of Physics, National University of Ireland Galway, University Road, Galway, Ireland
[10] Astronomy Department, Adler Planetarium and Astronomy Museum, Chicago, IL 60605, USA
[11] Department of Physics, Purdue University, West Lafayette, IN 47907, USA
[12] Department of Physics and Astronomy, Barnard College, Columbia University, NY 10027, USA; errando@astro.columbia.edu
[13] Department of Astronomy and Astrophysics, 525 Davey Lab, Pennsylvania State University, University Park, PA 16802, USA
[14] Institute of Physics and Astronomy, University of Potsdam, D-14476 Potsdam-Golm, Germany
[15] School of Physics and Astronomy, University of Minnesota, Minneapolis, MN 55455, USA
[16] Department of Physics and Astronomy, University of Iowa, Van Allen Hall, Iowa City, IA 52242, USA
[17] Department of Physics and Astronomy and the Bartol Research Institute, University of Delaware, Newark, DE 19716, USA; jholder@physics.udel.edu
[18] Physics Department, Columbia University, New York, NY 10027, USA
[19] [illegible]artment of Physics and Astronomy, DePauw University, Greencastle, IN 46135-0037, USA
[20] Department of Physics and Astronomy, University of Utah, Salt Lake City, UT 84112, USA
[21] Department of Physics and Astronomy, Iowa State University, Ames, IA 50011, USA
[22] Saha Institute of Nuclear Physics, Kolkata 700064, India
[23] Enrico Fermi Institute, University of Chicago, Chicago, IL 60637, USA
[24] [illegible]i Institute for Cosmological Physics, University of Chicago, Chicago, IL 60637, USA
[25] [illegible]ent of Physics, Anderson University, 1100 East 5th Street, Anderson, IN 46012, USA
[26] Department of Life and Physical Sciences, Galway-Mayo Institute of Technology, Dublin Road, Galway, Ireland
[27] School of Physics and Center for Relativistic Astrophysics, Georgia Institute of Technology, 837 State Street NW, Atlanta, GA 30332-[illegible]
[28] NASA/Goddard Space-Flight Center, Code 661, Greenbelt, MD 20771, USA
[29] Physics Department, California Polytechnic State University, San Luis Obispo, CA 94307, USA
[30] Department of Applied Physics and Instrumentation, Cork Institute of Technology, Bishopstown, Cork, Ireland
[31] Centre for Space Research, North-West University, Potchefstroom 2531, South Africa
[32] Laboratoire Leprince-Ringuet, École polytechnique, CNRS/IN2P3, Palaiseau, France; sfegan@llr.in2p3.fr
[33] Columbia Astrophysics Laboratory, Columbia University, New York, NY 10027, USA
[34] Max-Planck-Institut für Radioastronomie, Auf dem Hügel 69, D-53121 Bonn, Germany
[35] Astro Space Center of Lebedev Physical Institute, Profsoyuznaya Str. 84/32, 117997 Moscow, Russia
[36] Department of Physics, Purdue University, 525 Northwestern Avenue, West Lafayette, IN 47907, USA
[37] Pulkovo Astronomical Observatory, Pulkovskoe Chaussee 65/1, 196140 St. Petersburg, Russia
[38] Crimean Astrophysical Observatory, 98409 Nauchny, Crimea, Ukraine
[39] Steward Observatory, University of Arizona, Tucson, AZ 85721, USA

Received 2013 June 13; [illegible]2013 August 21; published 2013 September 27

ABSTRACT

We report the detection of a new TeV gamma-ray source, VER J0521+211, based on observations made with the VERITAS imaging atmospheric Cherenkov Telescope Array. These observations were motivated by the discovery of a cluster of >30 GeV photons in the first year of *Fermi* Large Area Telescope observations. VER J0521+211 is relatively bright at TeV energies, with a mean photon flux of $(1.93 \pm 0.13_{\rm stat} \pm 0.78_{\rm sys}) \times 10^{-11}$ cm^{-2} s^{-1} above 0.2 TeV during the period of the VERITAS observations. The source is strongly variable on a daily timescale across all wavebands, from optical to TeV, with a peak flux corresponding to ~0.3 times the steady Crab Nebula flux at TeV energies. Follow-up observations in the optical and X-ray bands classify the newly discovered TeV source as